

Electronic Supporting Information

Electric Field Modulated Peptide based Hydrogel Nanocatalyst

Jahnu Saikia^a, K.Dharmalingam^b, R. Anandalakshmi^b, Amay Sanjay Redkar^a, Venugopal T. Bhat^{c*} and Vibin Ramakrishnan^{a*}

Index

No	Content	Page No.
1.	Figure S1. Vial inversion test of the designed peptides	2
2	Figure S2. Streoselectivity of the EF treated and untreated hydrogels	3
3.	Figure S3. Characterization of gel forming peptides in presence and absence of electric field.	4
4.	Figure S4. FESEM analysis of the hydrogel forming peptides at different electric field strengths.	5
5.	Figure S5. Rheology of the peptide gels formed in presence and absence of EF	6
6.	Figure S6: Doxorubicin release assay	7
7.	Figure S7. Chiral chromatogram for the aldol products catalyzed by FFP hydrogel	8
8.	Figure S8. Chiral chromatogram for the aldol products catalyzed by PFF hydrogel	9
9.	Figure S9. Chiral chromatogram for the aldol products catalyzed by ffp hydrogel	10
10.	Figure S10. Chiral chromatogram for the aldol products catalyzed by pff hydrogel	11
11.	Figure S11. Chiral chromatogram for the aldol products catalyzed by Fmoc-FFP hydrogel	12
12.	Figure S12. Chiral chromatogram for the aldol products catalyzed by Fmoc-PFF hydrogel	13
13	FigureS13. Dipole moment of the peptides in water	14

1. Vial inversion test of the designed peptides

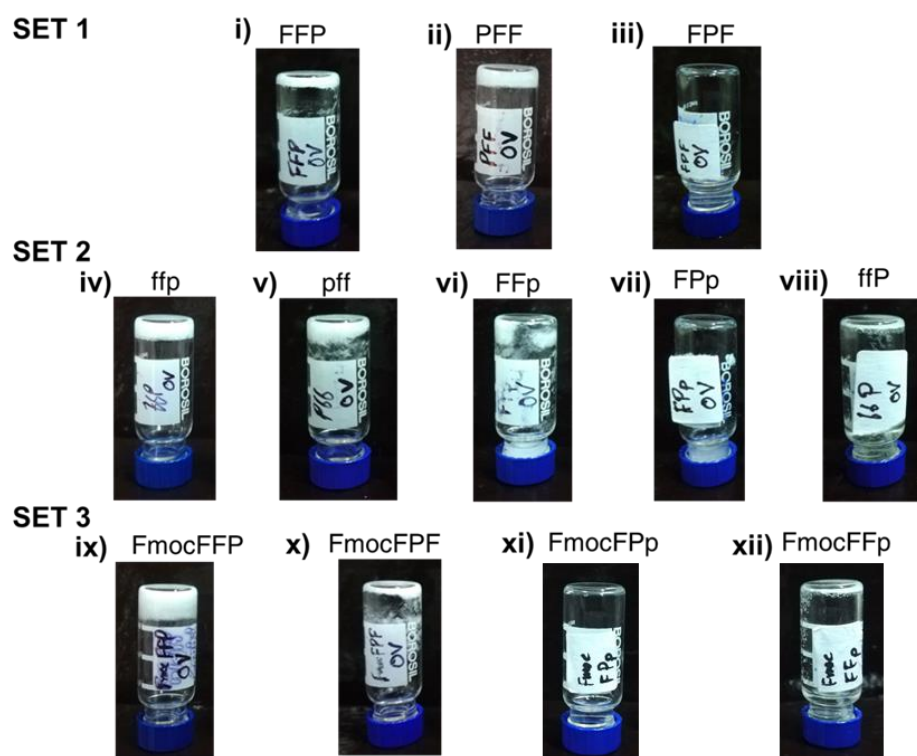


Figure S1: Vial inversion test confirming the hydrogel formation. A total of six peptides, FFP, PFF, ffp, pff, Fmoc-FFP, Fmoc-FFP out of twelve designed and synthesized peptides, formed white, opaque, self-supporting hydrogels in DMSO : phosphate buffer (1:10) following a temperature trigger.

2. Streoselectivity of the EF treated and untreated hydrogels

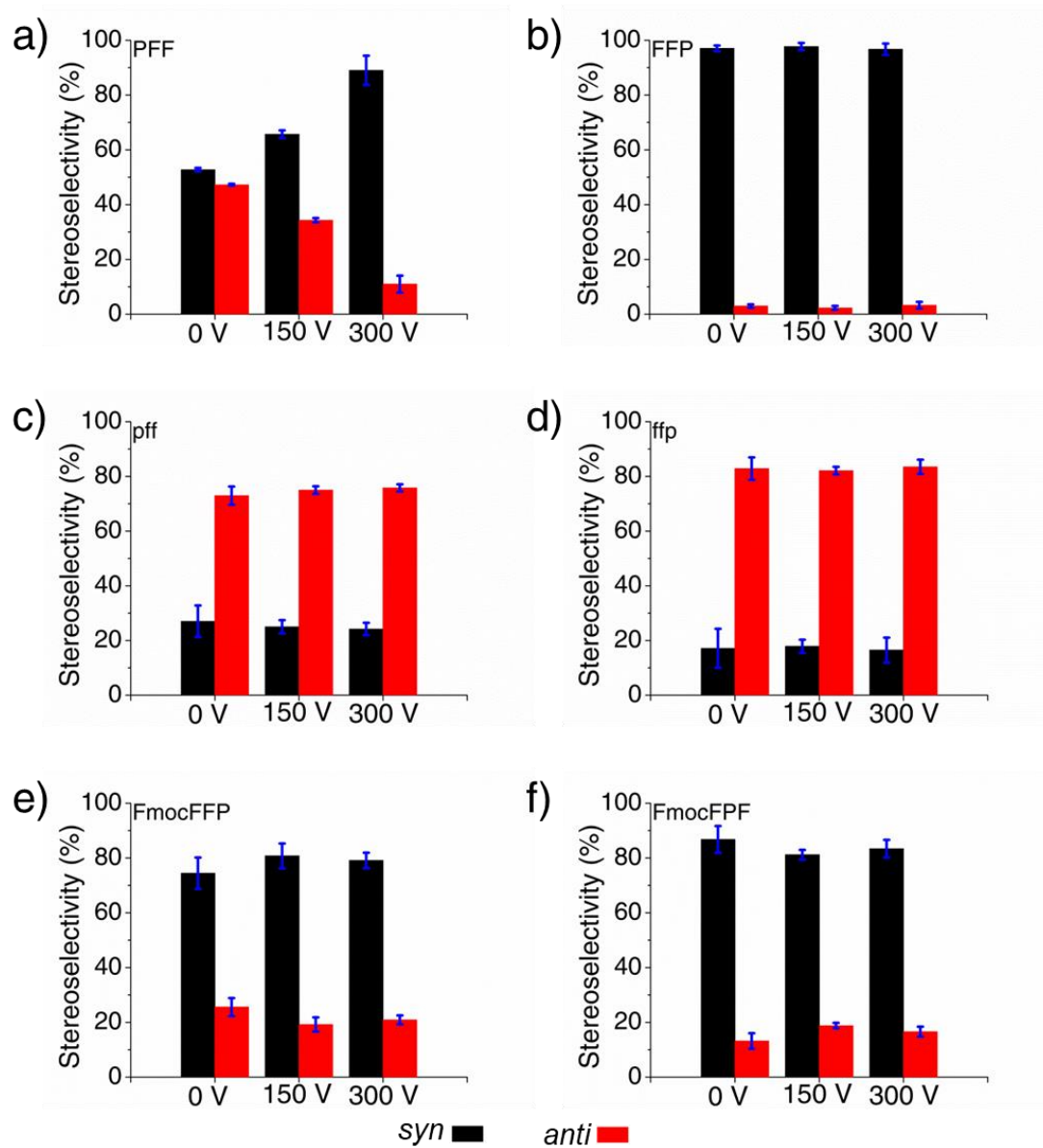


Figure S2: Representative streoselectivity of the EF treated and untreated hydrogels obtained from chiral HPLC chromatogram recorded at $\lambda=254\text{nm}$. The error bars represent the standard deviation of three independent observations.

3. Characterization of gel forming peptides in presence and absence of electric field.

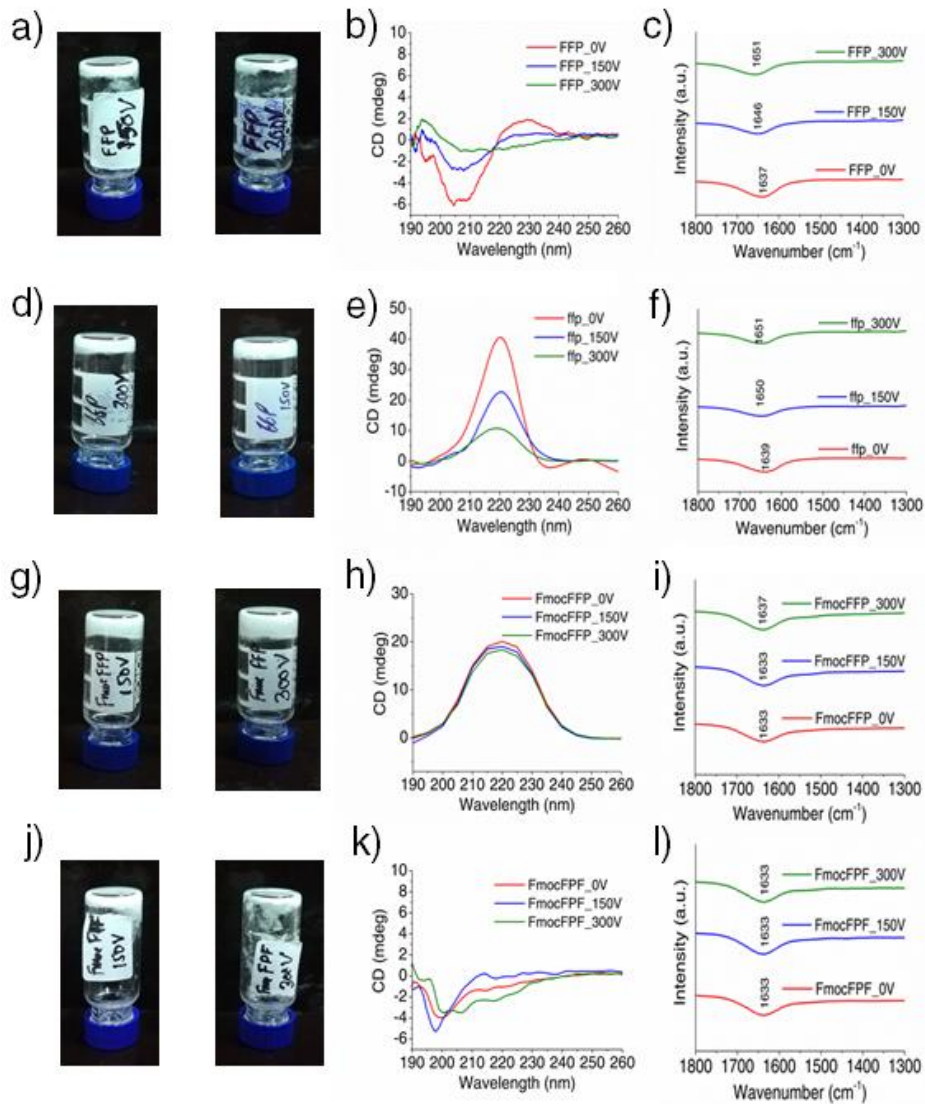
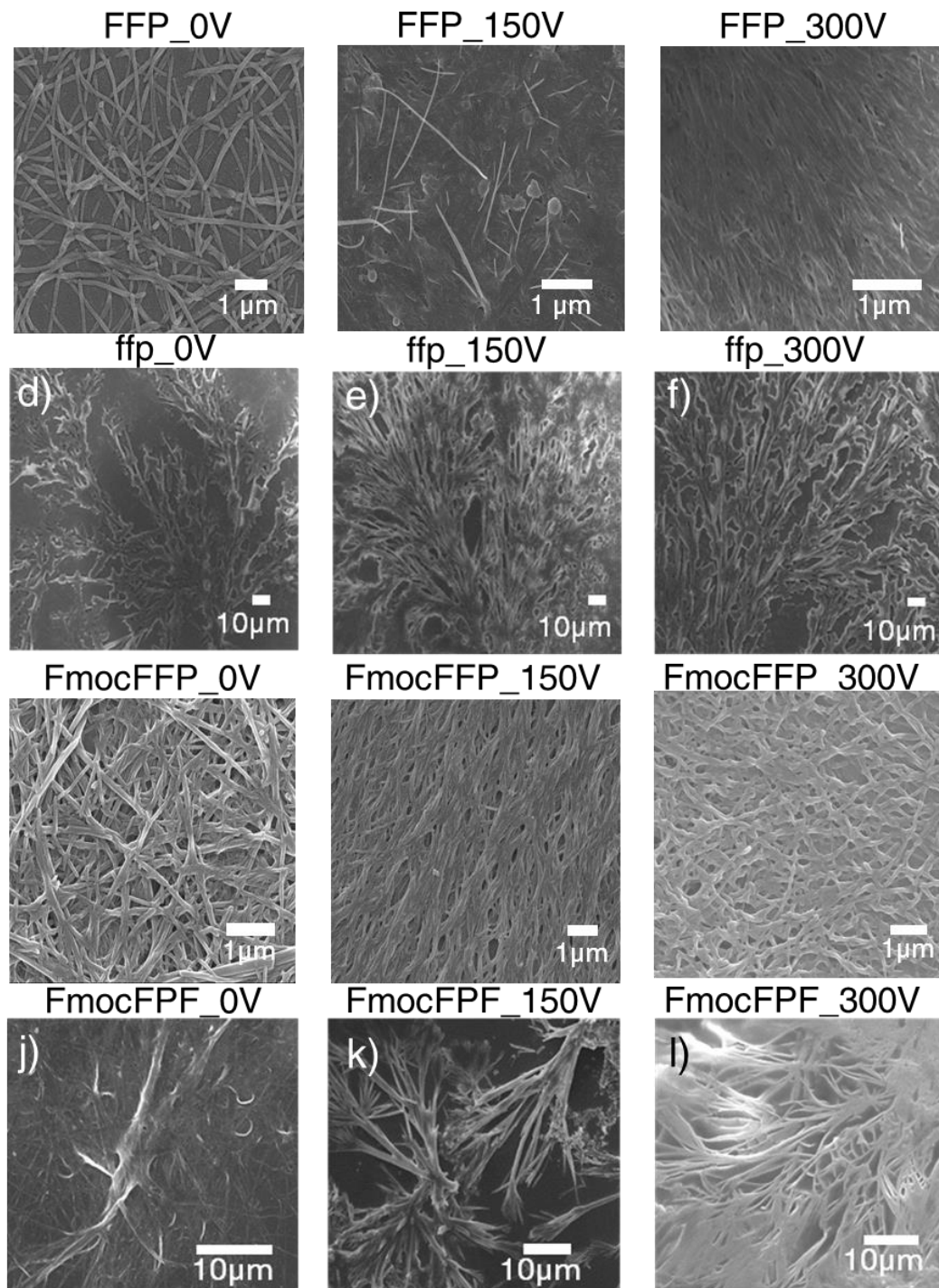


Figure S3. Characterization of the hydrogels. (a) Vial inversion test of FFP hydrogel formed in the presence of 150 and 300Vcm⁻¹ (b) CD spectra of FFP in 0 (red),150(blue) and 300Vcm⁻¹ (green). (c) FTIR spectra of FFP peptide in 0 (red),150(blue) and 300Vcm⁻¹ (green). (d) Vial inversion test of ffp hydrogel formed in the presence of 150 and 300Vcm⁻¹ (e) CD spectra of the ffp peptide in 0 (red),150(blue) and 300Vcm⁻¹ (green). (f) FTIR spectra of ffp peptide in 0 (red),150(blue) and 300Vcm⁻¹ (green).(g) Vial inversion test of Fmoc-FFP hydrogel formed in the presence of 150 and 300Vcm⁻¹ (h) CD spectra of Fmoc-FFP peptide in 0 (red),150(blue) and 300Vcm⁻¹ (green). (i)FTIR spectra of Fmoc-FFP peptide in 0 (red),150(blue) and 300Vcm⁻¹ (green). (j) Vial inversion test of Fmoc-PFP hydrogel formed in the presence of 150 and 300Vcm⁻¹ (k) CD spectra of Fmoc-PFP peptide in 0 (red),150(blue) and 300Vcm⁻¹ (green). (l) FTIR spectra of Fmoc-PFP peptide in 0 (red),150(blue) and 300Vcm⁻¹ (green).

4. FESEM analysis of the hydrogel forming peptides at different electric field strengths.



FigureS4. Morphological characterization of the gel forming peptide assemblies. FESEM images (a-c) of FFP hydrogel formed in 0, 150 and 300 Vcm^{-1} . The ffp hydrogel formed in 0, 150 and 300 Vcm^{-1} (d-f). Fmoc-FFP hydrogel formed in 0, 150 and 300 Vcm^{-1} (g-i) and Fmoc-FPF hydrogel formed in 0, 150 and 300 Vcm^{-1} after 12h of incubation under ambient conditions.

5. Rheology of the peptide gels formed in presence and absence of EF.

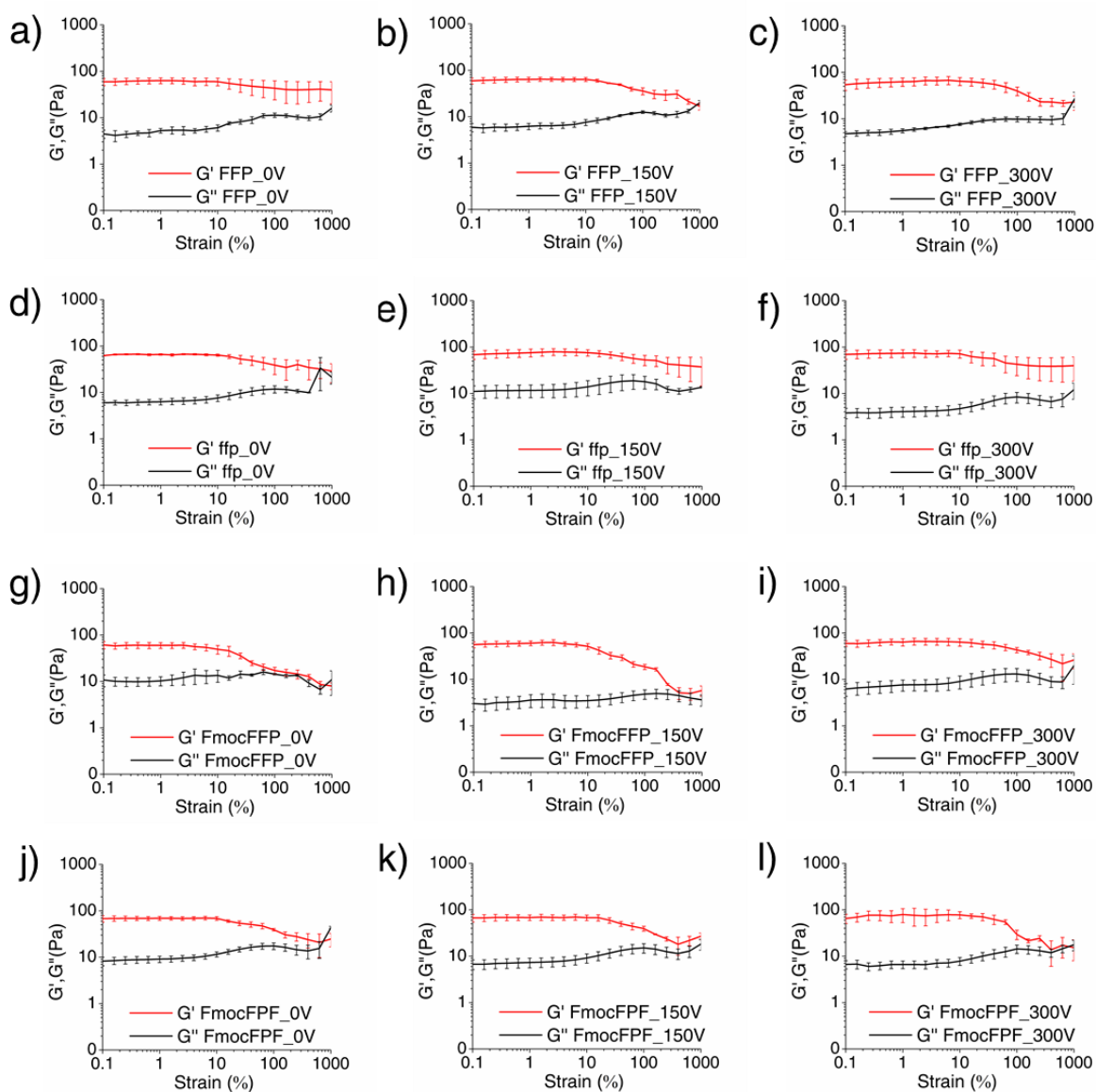


Figure S5. Amplitude sweep studies were carried out from 0.01 to 1000 % strain at a frequency of 10 rad s^{-1} at $25 \text{ }^\circ\text{C}$. Storage G' (red) and loss G'' (black) moduli of (a-c) FFP, (d-f) ffp (g-i) FmocFFP and (j-l) FmocFPF peptide hydrogels formed in the absence (0 Vcm^{-1}) and presence (150 and 300 Vcm^{-1}) of the external electric field. The error bars represent the standard errors of three independent observations.

6. Doxorubicin release assay

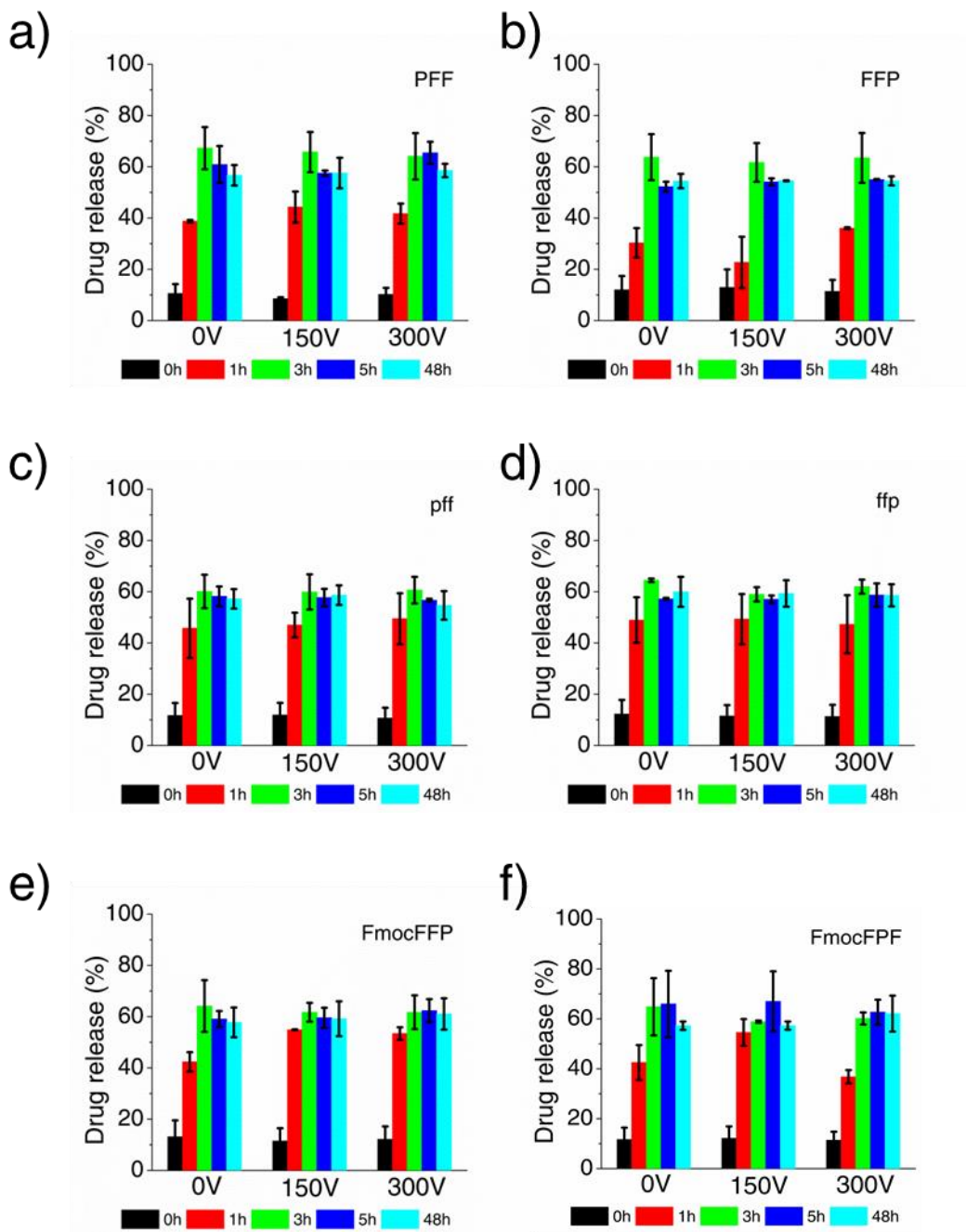
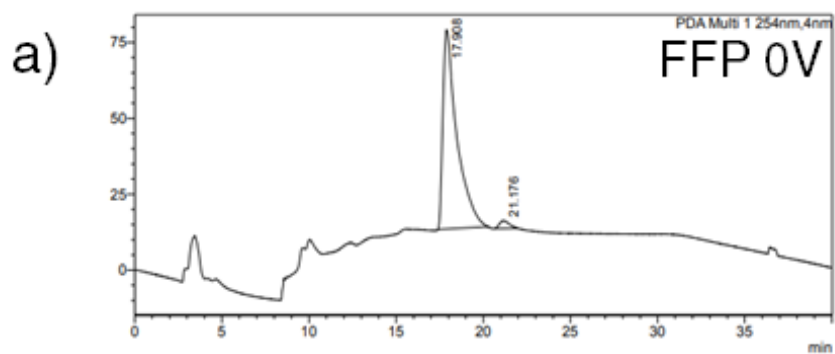
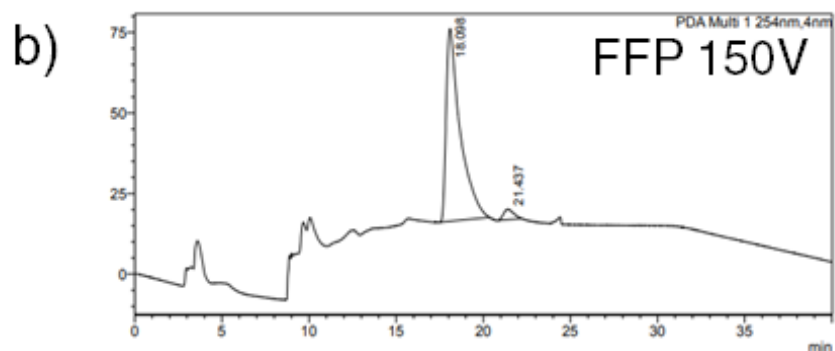


Figure S6: Doxorubicin release assay: Doxorubicin release kinetics from EF treated and untreated gels a) PFF b) FFP c) pff d) ffp e) FmocFFP and f) FmocFFP as determined by monitoring the absorbance at 490 nm. The error bars represent the standard deviation of three independent observations.



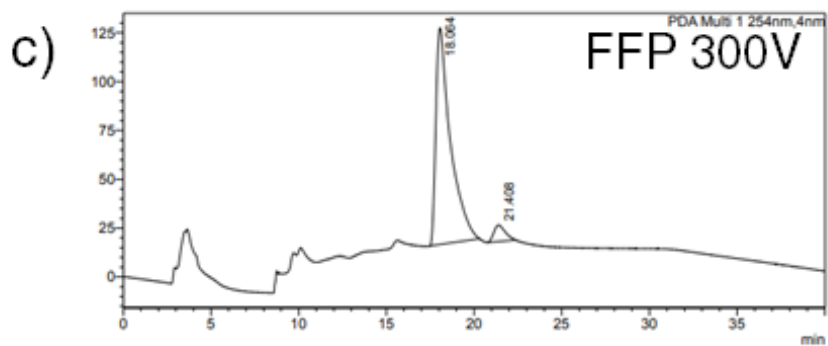
<Peak Table>

PDA Ch1 254nm			
Peak#	Ret. Time	Area	Area%
1	17.908	3667824	97.346
2	21.176	99984	2.654
Total		3767809	100.000



<Peak Table>

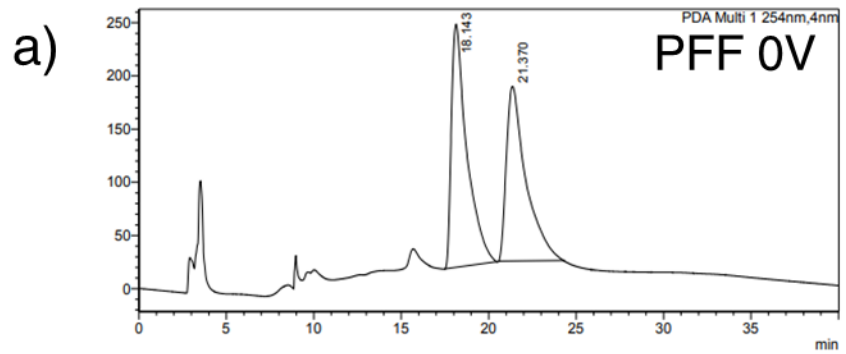
PDA Ch1 254nm			
Peak#	Ret. Time	Area	Area%
1	18.098	3334660	96.272
2	21.437	129118	3.728
Total		3463778	100.000



<Peak Table>

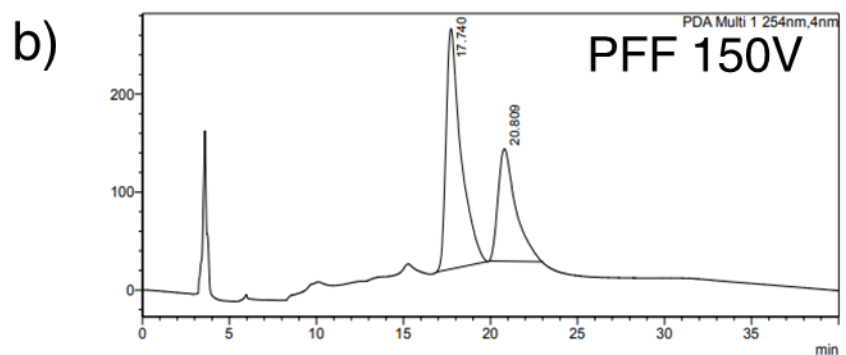
PDA Ch1 254nm			
Peak#	Ret. Time	Area	Area%
1	18.064	6423871	94.478
2	21.408	375481	5.522
Total		6799352	100.000

Figure S7. Chiral chromatogram for the aldol products catalyzed by FFP hydrogel formed in different EF strengths. Labeled peaks correspond to *syn* aldol (+) and *anti*-aldol (-). Ratio of integrals between the minor and the major enantiomers was used to determine the enantiomeric excess ee%.



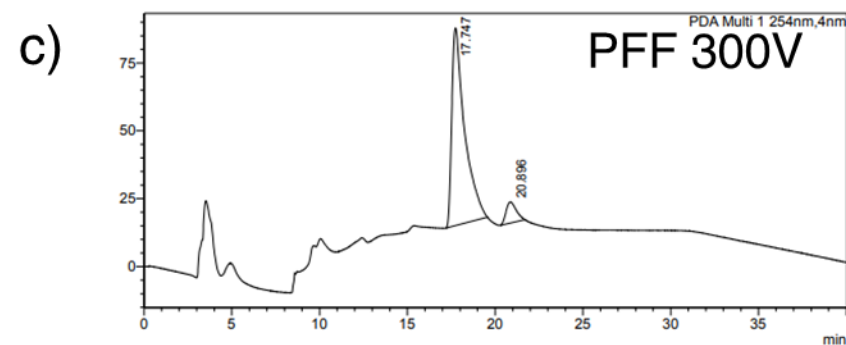
<Peak Table>

PDA Ch1 254nm			
Peak#	Ret. Time	Area	Area%
1	18.143	14060658	52.312
2	21.370	12817720	47.688
Total		26878378	100.000



<Peak Table>

PDA Ch1 254nm			
Peak#	Ret. Time	Area	Area%
1	17.740	14604138	64.195
2	20.809	8145352	35.805
Total		22749490	100.000



<Peak Table>

PDA Ch1 254nm			
Peak#	Ret. Time	Area	Area%
1	17.747	3704293	92.226
2	20.896	312250	7.774
Total		4016543	100.000

Figure S8. Chiral chromatogram for the aldol products catalyzed by PFF hydrogel formed in different EF strengths. Labeled peaks correspond to *syn* aldol (+) and *anti*-aldol (-). Integral ratios between the minor and the major enantiomers were used to determine the enantiomeric excess ee%.

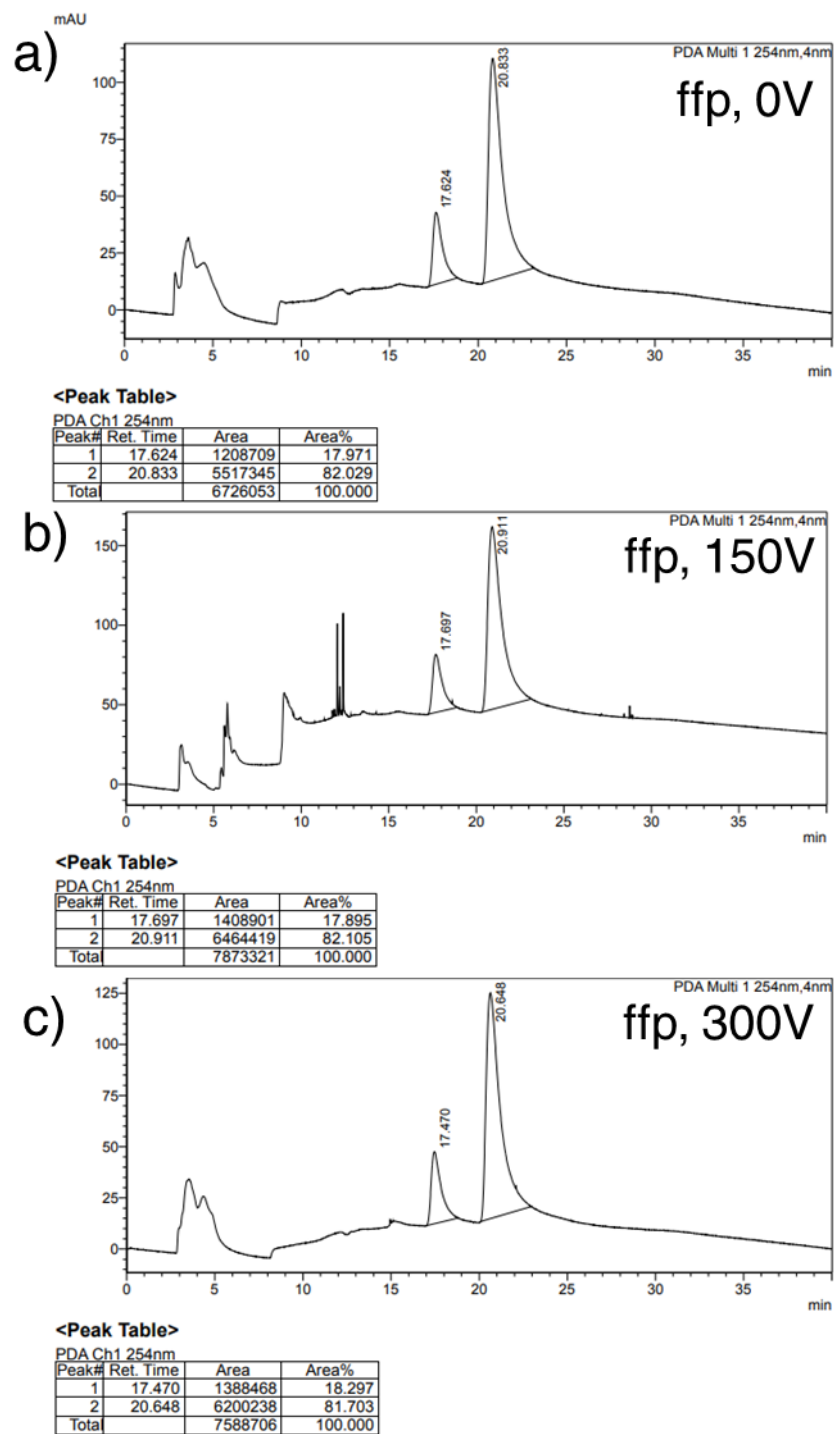


Figure S9. Chiral chromatogram for the aldol products catalyzed by **ffp** hydrogel formed in different EF strength. Labeled peaks correspond to *syn* aldol (+) and *anti*-aldol (-). Integral ratios between the minor and the major enantiomers were used to determine the enantiomeric excess ee%.

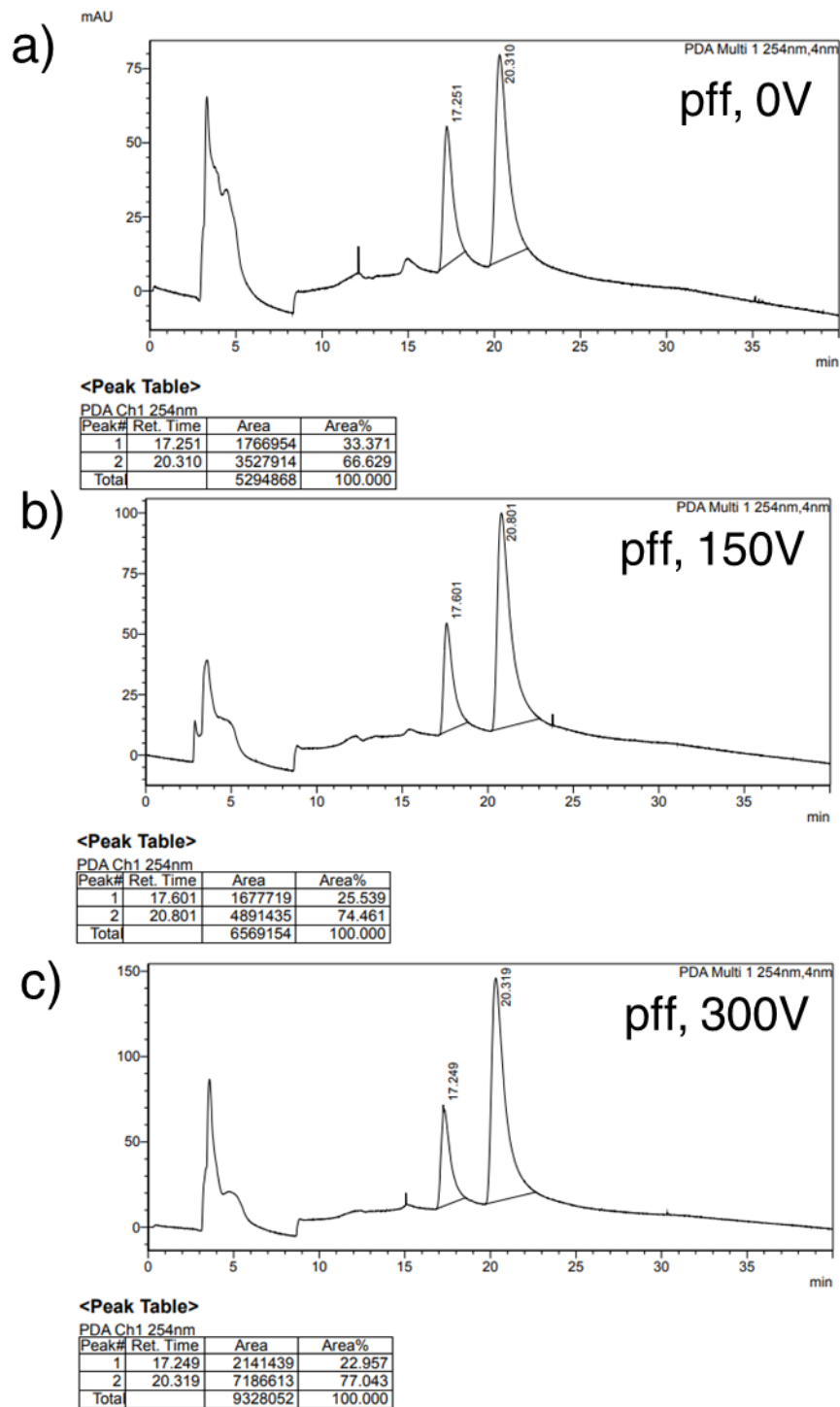


Figure S10. Chiral chromatogram for the aldol products catalyzed by **pff** hydrogel formed in different EF strength. Labeled peaks correspond to *syn* aldol (+) and *anti*-aldol (-). Integral ratios between the minor and the major enantiomers were used to determine the enantiomeric excess ee%.

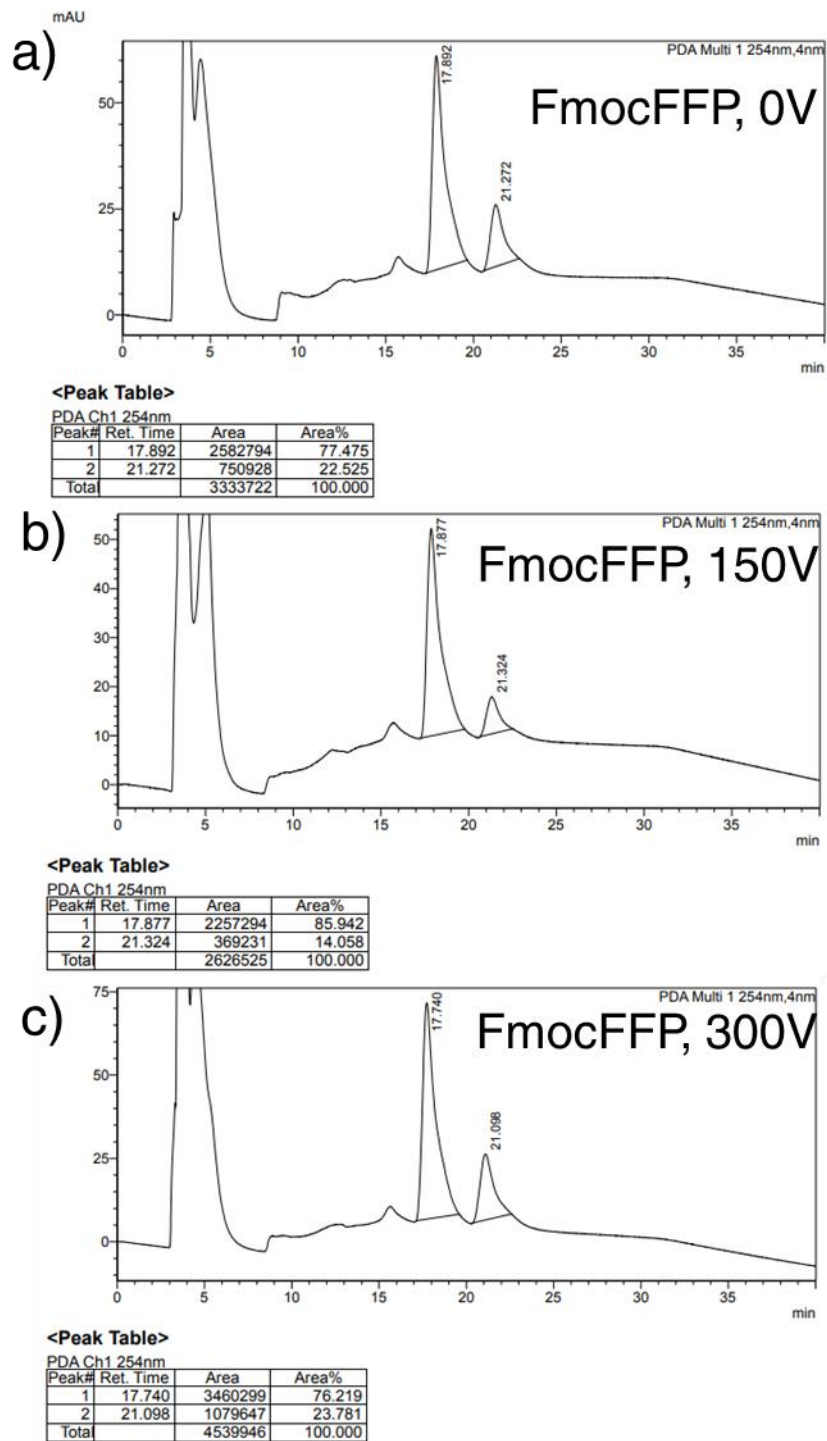


Figure S11. Chiral chromatogram for the aldol products catalyzed by **FmocFFP** hydrogel formed in different EF strength. Labeled peaks correspond to *syn* aldol (+) and *anti*-aldol (-). Integral ratios between the minor and the major enantiomers were used to determine the enantiomeric excess ee%.

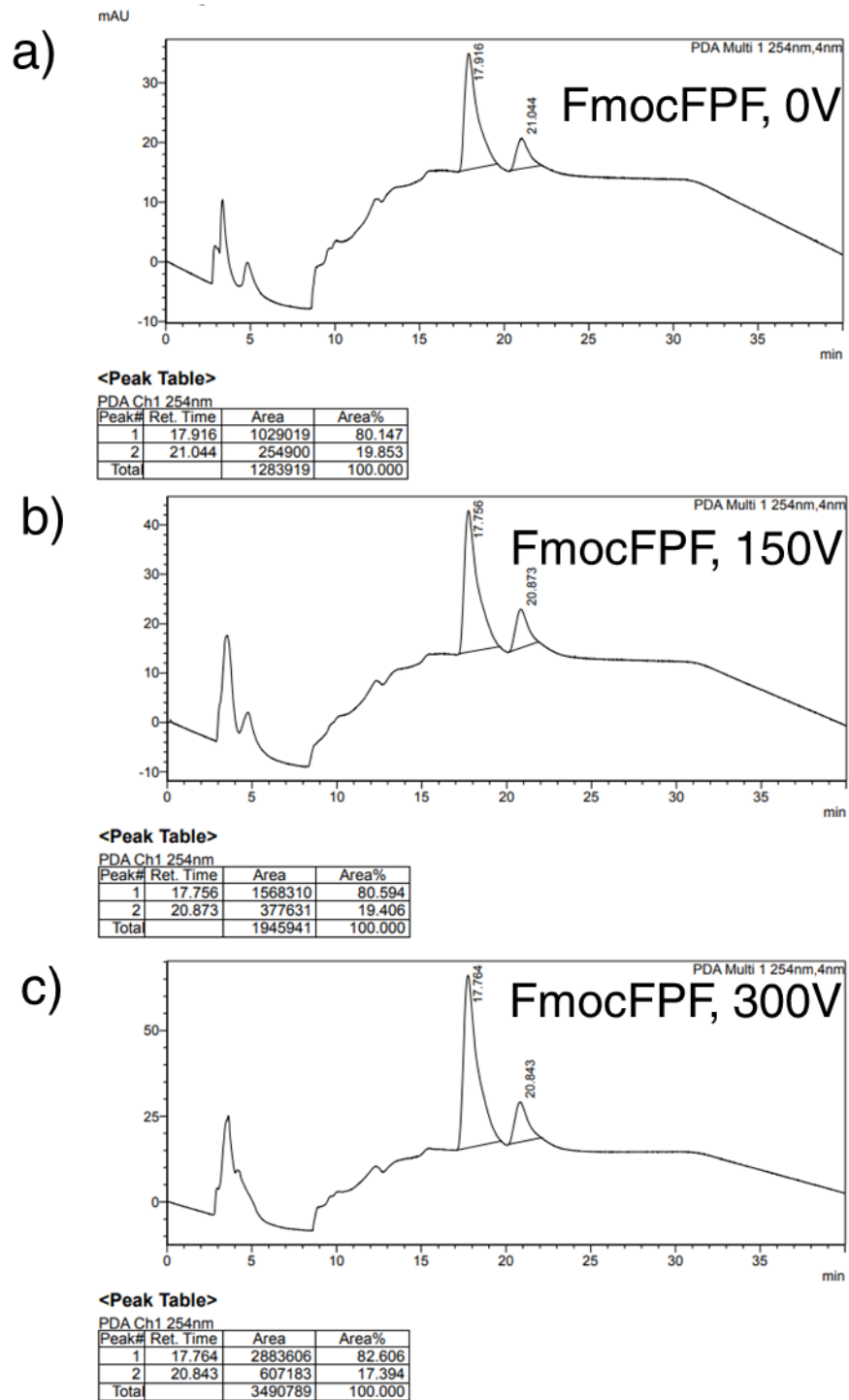


Figure S12. Chiral chromatogram for the aldol products catalyzed by **FmocFPF** hydrogel formed in different EF strength. Labeled peaks correspond to *syn* aldol (+) and *anti*-aldol (-). Integral ratios between the minor and the major enantiomers were used to determine the enantiomeric excess ee%.

7. Dipole moment of the peptides in water.

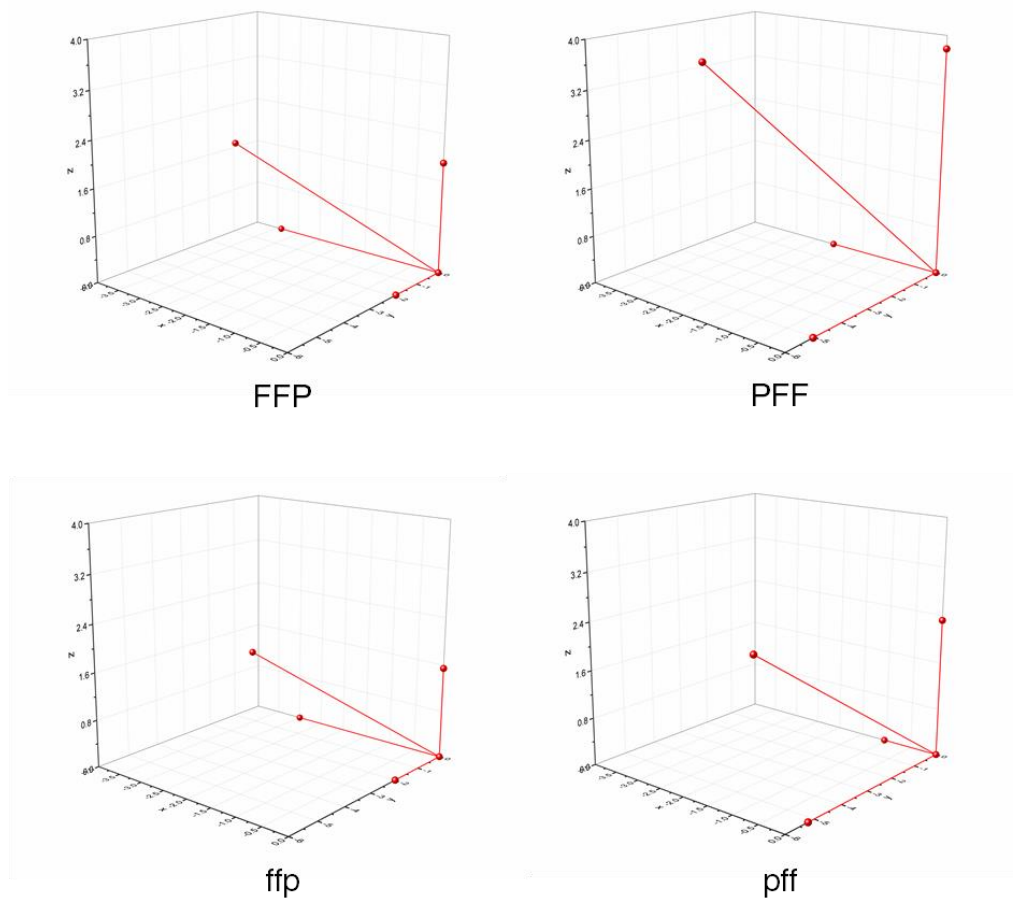


Figure S13: Dipole moment of the designed peptides in water. To study the dipole moment of the peptides in water, Molecular Dynamics (MD) simulations were performed with a GROMOS96 force field (54a7 parameter set) using GROMACS 5.0.4 package. Changes were made in the residue topology of the simulation tool, to incorporate the structural parameters of the D-amino acids. Each peptide was placed in a dodecahedron box with a spacing of 1.0 Å from the box edge. The system was solvated using the flexible SPC/E water model. The solvated system was neutralised to zero. Energy minimisation was carried out using the steepest descent until a tolerance of 1000 KJ mol⁻¹ nm⁻¹ was reached. Periodic boundary conditions were deployed in all the systems. The dipole moment of the peptides was calculated using gmx dipole for the energy minimised frame. $\langle M_i \rangle$, i for X, Y and Z axis, is the net vector in each frame. Dipole moments were calculated as the square root of the sum of the squares of $\langle M_i \rangle$.